Int. J. Multiphase Flow Vol. 5, pp. 395–412
Pergamon/Elsevier, 1979. Printed in Great Britain

THE FLOW OF CLOSELY FITTING PARTICLES IN TAPERED TUBES

HÜSNÜ TÖZEREN and RICHARD SKALAK
Department of Civil Engineering and Engineering Mechanics, Columbia University, New York, NY 10027, U.S.A.

(*Received* 30 *March* 1979; *in revised form* 4 *September* 1979)

Abstract—The flow of rigid spheres, truncated cones and elastic incompressible spheres in tapered tubes is investigated assuming that the Reynolds equation is valid in the fluid and the linear theory of elasticity is applicable in the solid. It is shown that leading terms in the asymptotic expansion of pressure drop in terms of minimum fluid film thickness for neutrally buoyant rigid spheres and truncated cones are of higher order of magnitude compared to the corresponding terms for the flow of these particles in circular cylindrical tubes. The effect of taper angle on pressure drop is reduced in the case of soft elastic particles because of particle deformations and significant velocities at the particle surface.

1. INTRODUCTION

In recent years, there have been a number of studies which model the blood flow in capillaries (see Goldsmith & Skalak 1975 for references). In these studies the blood cells are represented by rigid and deformable particles of various shapes. These studies generally assume steady state flow conditions and axisymmetrical configurations of the tubes and the particles. The present paper investigates some closely related problems of interest: (i) the flow of neutrally buoyant rigid spheres and truncated cones in tapered rubes, and (ii) the flow of elastic incompressible spheres in tapered tubes. The flows are unsteady because the geometry continually changes, but inertial effects will be neglected.

The first problem is a typical axisymmetric squeeze film problem which has been subject to numerous studies in the lubrication literature (see Desmond 1972). The cases of spherical, conical and truncated conical bearings were considered by Archibald (1956). He derived the equations giving the load carried by the bearing and settling time in terms of the speed of descent and some geometrical variables by integrating the Reynolds equation. In the case of neutrally buoyant particles treated in the present paper, the condition of zero drag on the particle must be satisfied also in addition to Reynolds equation. It can be used to eliminate leakback (which is equal to the discharge of the fluid observed relative to a reference frame fixed to the particle) leaving only pressure drop as an unknown. Then, integration of Reynolds equation yields the relation between the pressure drop, particle velocity and some geometrical and material constants. Results are given in section 2 as leading terms of the asymptotic expansions in minimum fluid film thickness.

The second problem considered in this paper is an extension of a recent study by Tözeren & Skalak (1978) on steady motion of elastic incompressible spheres in cylindrical tubes. In the present paper, the axisymmetric flow of elastic incompressible spheres in tapered tubes is investigated for several constant values of taper angle. The flow is assumed to be maintained by applying a constant pressure difference between upstream and downstream ends of the particle. The Reynolds equation is assumed to be valid in a thin lubcrication region between the closely fitting particle and the tube. The condition of zero drag on the particle is applied including the effects of squeezing motion due to relative inward movement of the tube wall. A series expansion is used to determine the particle deformations produced by the stresses applied along the particle surface using the formulation of Tözeren & Skalak (1978). The governing equations are nondimensionalized by introducing appropriate dimensionless variables and parameters. Solutions are obtained for several different values of dimensionless pressure drop and taper angle. Integration in time is started at relatively small values of diameter ratio (particle to tube

diameter) for which the particle deformations are small compared to fluid film thicknesses and velocities at the particle surface are negligible compared to particle velocity.

Finite difference formulae in time are used to approximate velocities along the particle surface. At a given instant, lubrication pressures, particle shape and its surface velocities are obtained by applying an iterative numerical procedure described in section 2. Numerical results are presented and discussed in section 3.

2. FORMULATION AND SOLUTIONS

The axisymmetric squeeze film problems for rigid neutrally buoyant truncated cones and spheres are treated first below. These permit asymptotic solutions for the pressure drop which drives the flow. Then the problem of the flow of elastic, incompressible spheres in a tapered tube is formulated and cast into dimensionless form. This problem is solved by numerical procedures outlined below and the results are discussed in section 3.

Rigid truncated cones

Consider the axisymmetric motion of a rigid truncated cone in a tapered tube with taper angle α (figure 1). The motion of this particle is assumed to be maintained by applying a constant pressure difference Δp between the upstream and the downstreams ends of the particles. Let U denote the particle velocity; h the fluid film thickness; r_1 and r_2 the radii of the tube at the upstream and downstream ends respectively. The Reynolds equation in one-dimension (i.e. Reynolds equation for infinitely long bearings) can be used here when the film thickness is small compared to particle radius. The Reynolds equation, referred to a reference frame fixed to the particle, is:

$$\frac{1}{6\mu}\frac{dp}{ds} = \frac{2Q}{h^3} - \frac{U\cos\alpha}{h^2} \qquad [2.1]$$

where p is the pressure and s is the distance of the point from the upstream end measured along the tube wall. The leakback Q is $1/2\pi r$ times the discharge of the fluid observed relative to the reference frame fixed to particle and given by:

$$2\pi rQ = \pi r^2 U - \pi r_1^2 \bar{V} \qquad [2.2]$$

where $\bar{V}$ is the average velocity at the upstream end of the particle ($s = 0$) and r is the tube radius at s ($r = r_1 - (\sin\alpha)s$). U and $\bar{V}$ are measured with the tube wall fixed and Q is a function of s.

The zero-drag condition can be derived by considering the equilibrium of a control volume including the particle bounded by the tube wall and two planes tangential to the particle at downstream and upstream faces:

$$\pi r_1^2 p_1 - \pi r_2^2 p_2 = -2\pi\cos\alpha\int_0^l r\tau\,ds + 2\pi\sin\alpha\int_0^l rp\,ds \qquad [2.3]$$

where l is the particle length measured parallel to s. The l.h.s. of [2.3] gives the force due to pressures acting over the downstream and upstream faces of the control volume. The second term of the r.h.s. of [2.3] is the component of pressure resultant on control volume in z-direction. The first term of the r.h.s. of [2.3] is the resultant of shear stresses on the tube wall in the z-direction. The shear stress τ acting along the tube wall can be expressed as

$$\tau = \frac{1}{2}\frac{dp}{ds}h - \frac{\mu U\cos\alpha}{h}. \qquad [2.4]$$

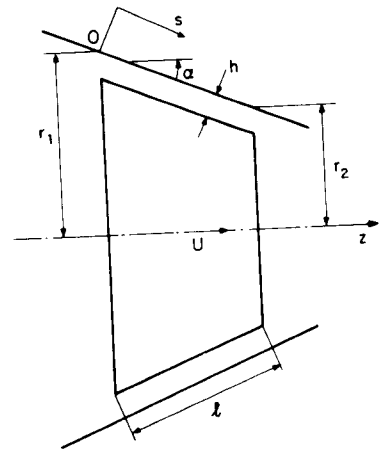

Figure 1. Flow of a neutrally buoyant rigid truncated conical particle through a tapered tube.

Equation [2.3] may be simplified by integrating the second term of the r.h.s. of [2.3] by parts:

$$\int_{r_1}^{r^2} r^2 \frac{dp}{dr}\, dr = 2\cos\alpha \int_0^l r\tau\, ds. \qquad [2.5]$$

Equations [2.1], [2.4] and [2.5] are non-dimensionalized by introducing the following dimensionless variables:

$$P = p/(\mu U/r_1), \quad R = r/r_1, \quad S = s/r_1$$
$$V = \bar{V}/U, \quad H = h/r_1, \quad T = \tau/(\mu U/r_1). \qquad [2.6]$$

Equations [2.1], [2.4] and [2.5] in dimensionless forms are:

$$\frac{dP}{dS} = \frac{6}{H^3}\left(R - \frac{V}{R}\right) - \frac{6\cos\alpha}{H^2} \qquad [2.7]$$

$$T = \frac{1}{2}\frac{dP}{dS}H - \frac{\cos\alpha}{H} \qquad [2.8]$$

$$\int_1^{R_2} R^2 \frac{dP}{dR}\, dR = 2\cos\alpha \int_0^L RT\, dS. \qquad [2.9]$$

It will be assumed that P, T and V possess the following asymptotic expansions in H as $H \to O$:

$$P = \frac{1}{H^3}(P_0 + P_1 H + O(H^2)) \qquad [2.10]$$

$$T = \frac{1}{H^2}(T_0 + T_1 H + O(H^2)) \qquad [2.11]$$

$$V = V_0 + V_1 H + O(H^2). \qquad [2.12]$$

Equations [2.10] and [2.11] follow directly from [2.7] and [2.8]. The power series expansion for V will not contain any singular terms in H. Hence it is given as a regular series expansion in terms of H in [2.12].

Substituting [2.10]–[2.12] into [2.7]–[2.9] and collecting the same order terms in H the

differential equations for the zero order terms are obtained:

$$\frac{dP_0}{dS} = 6\left(R - \frac{V_0}{R}\right) \tag{2.13}$$

$$\int_1^{R_2} R^2 \frac{dP_0}{dR}\, dR = 0. \tag{2.14}$$

Substituting [2.13] into [2.14] and carrying out the integration, V_0 is determined in terms of geometrical parameters:

$$V_0 = \frac{1 + R_2^2}{2}. \tag{2.15}$$

Using [2.15] in [2.13] and integrating this ordinary differential equation:

$$\Delta P_0 = \frac{3}{\sin \alpha}[(R_2^2 - 1) - (1 + R_2^2) \ln R_2] \tag{2.16}$$

where ΔP_0 is the leading term of the asymptotic expansion of dimensionless pressure drop as $H \to O$. Dimensional equations for Δp and $\bar{V}$ considering only the leading terms:

$$\bar{V} \approx \frac{r_1^2 + r_2^2}{2r_1^2} U \tag{2.17}$$

$$\Delta p \approx \frac{3\mu U}{\sin \alpha h^3}\left[(r_2^2 - r_1^2) - (r_2^2 + r_1^2) \ln \frac{r_2}{r_1}\right]. \tag{2.18}$$

Rigid spheres

A similar asymptotic expansion asymptotic expansion as outlined above for cones can be developed for the case of rigid spheres (figure 2). The fluid film thickness h measured perpendicular to the tube wall and s is the distance of the points on the tube from the point O where h attains its minimum value h_0.

The Reynolds equation is

$$\frac{1}{6\mu}\frac{dp}{ds} = \frac{1}{h^3}\left(Ur - \bar{V}\frac{r_0^2}{r}\right) - \frac{U \cos \alpha}{h^2} \tag{2.19}$$

where $\bar{V}$ = mean velocity at $s = 0$ and r_0 = tube radius at $s = 0$. The zero drag condition is given by:

$$\int_{s_1}^{s_2} r^2 \frac{dp}{ds}\, ds = 2 \cos \alpha \int_{s_1}^{s_2} r\tau\, ds \tag{2.20}$$

where τ is given by [2.4] and the integration limits s_1 and s_2 are coordinates of upstream and downstream ends of the particle.

The following dimensionless variables are defined:

$$P = p/(\mu U/r_0), \quad R = r/r_0, \quad S = s/a, \quad V = \bar{V}/U,$$
$$H = h/h_0, \quad T = \tau/(\mu U/r_0) \quad \text{and} \quad \epsilon = h_0/r_0. \tag{2.21}$$

Equations [2.19], [2.4] and [2.20] in dimensionless form are:

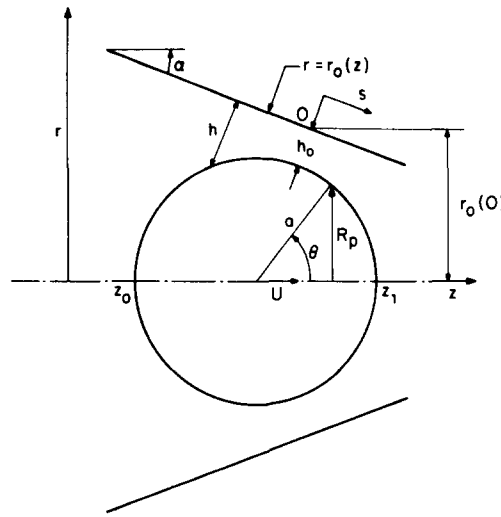

Figure 2. Flow of a neutrally buoyant spherical particle through a tapered tube.

$$\frac{dP}{dS} = 6\left(\frac{a}{r_0}\right)\left[\frac{(R - V/R)/H^3}{\epsilon^3} - \frac{\cos\alpha/H^2}{\epsilon^2}\right] \tag{2.22}$$

$$\int_{S_1}^{S_2} R^2 \frac{dP}{dS}\, dS = 2\cos\alpha\left(\frac{a}{r_0}\right)\int_{S_1}^{S_2} RT\, dS \tag{2.23}$$

$$T = \frac{H\dfrac{dP}{dS}}{2\left(\dfrac{a}{r_0}\right)}\epsilon - \frac{\cos\alpha/H}{\epsilon}. \tag{2.24}$$

From [2.22] it can be seen that the significant buildup of pressures takes place in a central region in the vicinity of origin for which $S = O(1)$ and $H = O(1)$. The pressure gradient outside this region is negligible since $H \gg 1$ when $S = O(1)$. The fluid film thickness h is approximated by a second order polynomial in this central region where $S = O(1)$:

$$h = h_0 + \frac{s^2}{2a}. \tag{2.25}$$

The effect of replacement of circle by parabola is discussed in detail by Cameron (1966).

Now assume that P, T and V may be expressed in the form of the following asymptotic expansions in ϵ:

$$P = \frac{1}{\epsilon^n}(P_0 + P_1\epsilon + O(\epsilon^2)) \tag{2.26}$$

$$T = \frac{1}{\epsilon^{n-1}}(T_0 + T_1\epsilon + O(\epsilon^2)) \tag{2.27}$$

$$V = V_0 + V_1\epsilon + O(\epsilon^2) \tag{2.28}$$

where n is some integer.

As ϵ tends to zero, the average velocity at $s = 0$, $\bar{V}$, must approach to the particle velocity, U. Hence V_0 in [2.30] must be equal to unity. Under this condition and using [2.25], an analysis of [2.22] and [2.23] shows that it is proper to take n equal to 2 in [2.27] and [2.28]. The assumption of these specific forms for asymptotic series of P and T will be subject to verification in later steps when we attempt to determine the explicit forms of the coefficients of

the leading terms, P_0 and T_0. The approximation of film thickness by [2.25] is sufficient to determine these leading terms exactly (see Cameron 1966).

The differential equations for the leading terms of pressure are

$$\frac{dP_0}{dS} = 6\left(\frac{a}{r_0}\right)\left\{\frac{R-(1/R)}{\epsilon H^3} - \frac{V_1}{RH^3} - \frac{\cos\alpha}{H^2}\right\} \tag{2.28}$$

$$\int_{S_0}^{S_1} R^2 \frac{dP_0}{dS}\, dS = 0. \tag{2.29}$$

Substitution of dP_0/dS into [2.29] and use of $R = 1 - [(a \sin\alpha)/r_0]S$ yield:

$$\int_{S_0}^{S_1} R^2 \frac{dP_0}{dS}\, dS = \int_{S_0}^{S_1} \left(3\left(\frac{a}{r_0}\right)^2 \sin^2\sigma \frac{S^2}{\epsilon H^3} - \frac{V_1}{H^3} - \frac{\cos\alpha}{H^2}\right) dS = 0. \tag{2.30}$$

In [2.30] terms involving odd powers of S are neglected since their contribution to the integral is of smaller order of magnitude than the terms given in the integral. Equation [2.25] in dimensionless form is:

$$H = 1 + \left(\frac{a}{r_0}\right)\frac{S^2}{2\epsilon} \tag{2.31}$$

or

$$S = \pm\left(\frac{2(H-1)\epsilon}{a/r_0}\right)^{1/2}. \tag{2.32}$$

Substituting [2.32] into [2.30] and calculating the integrals of the several terms give:

$$\begin{aligned}
\int_{S_0}^{S_1} \frac{dS}{H^2} &= \left(\frac{2\epsilon}{a/r_0}\right)^{1/2} \int_1^{(a/r_0)(1/2\epsilon)} \frac{dH}{\sqrt{(H-1H^2)}} + O(\epsilon^{1/2}) \\
&= \frac{\pi}{2}\left(\frac{a}{r_0}\right)^{-(1/2)} \sqrt{\epsilon} + O(\sqrt{\epsilon}) \\
\frac{1}{\epsilon}\int_{S_0}^{S_1} \frac{S^2\, dS}{H^3} &= \frac{\pi}{4}\sqrt{2}\left(\frac{a}{r_0}\right)^{-(3/2)} \sqrt{\epsilon} + O(\sqrt{\epsilon}) \\
\int_{S_0}^{S_1} \frac{dS}{H^3} &= \frac{3\pi}{8}\left(\frac{a}{r_0}\right)^{-(3/2)} \sqrt{\epsilon} + O(\sqrt{\epsilon}).
\end{aligned} \tag{2.33}$$

Substituting [2.33] into [2.30],

$$V_1 = \left(-\frac{4}{3}\cos\alpha + 2\left(\frac{a}{r_0}\right)\sin^2\alpha\right) \tag{2.34}$$

and substituting V_1 in [2.28], using same approximations and integrating between S_0 and S_1,

$$\Delta P = 6\sqrt{2}\pi\left(\frac{a}{r_0}\right)^{3/2} \sin^2\alpha\epsilon^{-(3/2)} + o(\epsilon^{-(3/2)}). \tag{2.35}$$

The average velocity $\bar{V}$ and pressure drop Δp in terms of dimensional variables are

$$\bar{V} \approx \left\{1 + \frac{h_0}{r_0}\left(-\frac{4}{3}\cos\alpha + 2\sin^2\alpha\left(\frac{a}{r_0}\right)\right)\right\} U \tag{2.36}$$

$$\Delta p \approx \frac{6\sqrt{2}\pi\mu U}{h_0^{3/2}}\left(\frac{a}{r_0}\right)^{3/2} r_0^{1/2} \sin^2\alpha. \tag{2.37}$$

This completes the asymptotic analysis for rigid cones and spheres in tapered tubes.

Elastic incompressible spheres

Consider the axisymmetric motion of an elastic incompressible particle of initially spherical shape through a tapered tube in which the flow is assumed to be maintained by applying a constant pressure difference Δp between the upstream and downstream ends of the particle. The taper angle α is assumed to be small. The center of the particle translates with a velocity U which is a function of time (figure 2). The same notation is used for the variables involving geometry and material properties of the fluid as in the case of rigid spheres considered above except that the fluid film thickness h is measured along r axis (perpendicular to axis of the tube) in the present case. Although the flow is unsteady, it is assumed that the inertial terms are negligible and that the Navier–Stokes equations may be reduced to the Stokes equations:

$$\mu \nabla^2 v_i = \frac{\partial p}{\partial x_i} \tag{2.38}$$

where v_i is the velocity vector and p is the pressure in the fluid. The equation of continuity valid in the fluid is:

$$\frac{\partial v_i}{\partial x_i} = 0. \tag{2.39}$$

The Stokes equations [2.38] and equation of continuity [2.39] can be reduced to a Reynolds equation under the assumption that the clearance between the particle and the tube is small compared to the dimensions of the particle. A cylindrical coordinate system (r, θ, z) which is fiexed relative to the particle is used to express the field equations in the fluid (figure 2). The Reynolds equation is developed by integrating [2.38] and [2.39] under the assumption that p does not vary with r:

$$\frac{dp}{dz} = r_0(z_0)Q - U\left[\frac{1}{2}r_0^2 + \frac{2r_0h - h^2}{4\ln\left(1 - \frac{h}{r_0}\right)}\right]\left[\frac{2r_0h - h^2}{16\mu}\right]^{-1}$$

$$\times \left[2r_0^2 - 2r_0h + h^2 + \frac{2r_0h - h^2}{\ln\left(1 - \frac{h}{r_0}\right)}\right]^{-1}. \tag{2.40}$$

The choice of z rather than s as the longitudinal variable is permissible since it is assumed that α is a small angle. There are some differences between [2.40] and Reynolds equation developed for steady-state conditions (Fitz-Gerald 1969). Firstly, in the present case the pressure p and fluid film thickness h are time-dependent variables. Secondly, the leakback Q in [2.40] at any instant t is a function of z due to nonuniform tube geometry and the velocities at the particle surface. The value of $2\pi r_0(z_0)Q$ is the discharge at z observed relative to (r, θ, z) coordinate system. The equation of conservation of mass (figure 3) gives

$$2\pi r_0(z_0)Q = 2\pi r_0(z_0)Q(z_0) - \int_{S_p} v_i n_i \, dS - \pi U(r_0^2(z_0) - r_0^2) \tag{2.41}$$

where z_0 is the coordinate of upstream end of the particle, r_0 is the radius of the tube as a function of z, S_p is the surface of the particle, n_i is the unit normal vector on S_p and v_i is the velocity on S_p.

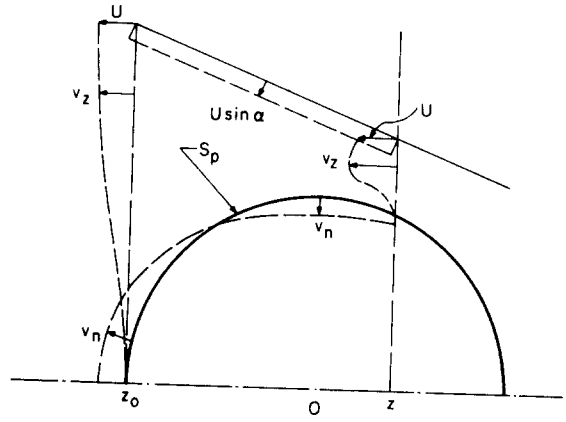

Figure 3. Sketch of velocity distributions along the boundaries of a control volume bounded by the tube wall, particle surface and two planes perpendicular to the axis of the tube at z_0 and z.

The condition of zero drag on the particle is:

$$\pi(p(z_0)r_0^2(z_0) - p(z_1)r_0^2(z_1)) = 2\pi \int_{z_0}^{z_1} r_0 p \tan\alpha \, dz - 2\pi \int_{z_0}^{z_1} r_0 \tau_{rz}|_{r=r_0} dz \qquad [2.42]$$

where z_0 and z_1 are the z coordinates of the upstream and the downstream ends of the particle or τ_{rz} is the shear stress in the lubrication layer.

The preceding equations are nondimensionalized by introducing the following dimensionless variables and parameters:

$$\bar{v}_i = \frac{v_i}{U}, \quad \bar{t} = \frac{t}{\mu/G}, \quad \bar{r}_i = \frac{r_i}{a}, \quad \bar{h} = \frac{h}{r_0(z_0)},$$

$$\bar{r}_0 = \frac{r_0}{r_0(z_0)}, \quad \bar{\sigma}_{ij} = \frac{\sigma_{ij}}{G}, \quad \bar{p} = \frac{p}{G}, \quad \bar{u}_i = \frac{u_i}{a}$$

where G is the shear modulus of the elastic material, and u_i is the displacement in the elastic particle. $A = \mu Ua/Gr_0^2(z_0)$ = velocity parameter; $\lambda_i = a/r_0(0)$ = initial diameter ratio; $\lambda_u = a/r_0(z_0)$ = diameter ratio obtained using $r_0(z_0)$; and rather than $r_0(0)$; $C = 2Q/Ur_0(z_0)$ = leakback parameter. Equations [2.41], [2.40] and [2.42], in terms of these dimensionless variables, are

$$C = C_0 - \frac{\lambda_u^2}{\pi} \int_{\bar{S}_p} \bar{v}_i n_i \, d\bar{S} - 1 + \bar{r}_0^2 \qquad [2.43]$$

$$\frac{d\bar{p}}{d\bar{z}} = 8A \left[C - \left(\bar{r}_0^2 + \frac{2\bar{r}_0\bar{h} - \bar{h}^2}{2\ln\left(1 - \frac{\bar{h}}{\bar{r}_0}\right)} \right) \right] [\bar{h}(2\bar{r}_0 - \bar{h})]^{-1} \times \left[2\bar{r}_0^2 - 2\bar{r}_0\bar{h} + \bar{h}^2 + \frac{2\bar{r}_0\bar{h} - \bar{h}^2}{\ln\left(1 - \frac{\bar{h}}{\bar{r}_0}\right)} \right]^{-1} \qquad [2.44]$$

$$\bar{p}(\bar{z}_0) - \bar{p}(\bar{z}_1)\bar{r}_0^2(\bar{z}_1) = 2\lambda_u \tan\alpha \int_{\bar{z}_0}^{\bar{z}_1} \bar{r}_0 \bar{p} \, d\bar{z} - 2\lambda_u \int_{\bar{z}_0}^{\bar{z}_1} \bar{r}_0 \bar{\tau}_{rz} \, d\bar{z}. \qquad [2.45]$$

The equations governing the motion of elastic incompressible particles are (neglecting the acceleration terms):

$$G\nabla^2 u_i = \frac{\partial p}{\partial x_i}, \quad \frac{\partial u_i}{\partial x_i} = 0. \qquad [2.46]$$

When the surface tractions are specified on the particle surface, the displacements throughout the particle can be obtained by using a series expansion in spherical harmonics developed by Lamb (1945). The application of this solution to the problem of steady flow of elastic spheres in tubes is discussed by Tözeren & Skalak (1978). The same formulation is used in the present case also since the inertial terms are assumed to be negligible.

The governing equations in the fluid and the solid are coupled by the requirements that: (i) the stress vector is continuous across the fluid–solid interface and (ii) the fluid film thickness is dependent on the deformations of the particle along the surface.

Numerical solutions of [2.43]–[2.46] are obtained for several values of cone angle α and pressure drop $\Delta\bar{p}$ by the numerical procedure described below.

Suppose that a certain past time instants $t_0, t_1, \ldots . t_{n-1}$ the solutions for particle deformations, the velocity parameter A and the location of the center of the particle are known. If an estimate of particle deformations and the parameter A can be found in the current time t_n, then the location of the center of the particle z_n at t_n may be estimated:

$$z_n = \int_{t_0}^{t_n} U \, dt = a \int_{\bar{t}_0}^{\bar{t}_n} A\lambda_u^{-2} \, d\bar{t}. \qquad [2.47]$$

The velocity at any point can also be estimated by using finite difference formulae.

$$\bar{v}_i = \frac{du_i}{dt} \Big/ U = \frac{\lambda_u^2}{A} \frac{d\bar{u}_i}{d\bar{t}}. \qquad [2.48]$$

Then [2.43]–[2.45] are solved to obtain lubrication pressures and shear stresses for the new position, particle shape and velocities at time t_n. The additional displacements of the particle due to the difference of these computed surface stresses from the stresses that give the estimate of displacements are found by using the series solution for diplacements. Now A and z_n are held fixed and the approximation to surface displacements and velocities are updated by using the previous estimates and additional displacements. This iterative cycle is repeated until the additional displacements become sufficiently small compared to the magnitude of the current approximation to displacements.

Further iterations on A are required if the integral of Reynolds equation [2.44] between $\bar{z}_0$ and $\bar{z}_1$ is not equal to the specified value of pressure drop $\Delta\bar{p}$. No more than three iterations on A and fifteen for displacements are needed to obtain three significant figures in these variables.

The integration in time is started at small values of λ_i for which the minimum film thickness is much larger than the particle deformations and surface velocities of the particle are negligible compared to $U \tan\alpha$. After calculating the solutions for a few initial time steps, a backward difference formula is used to approximate the surface velocities at current step.

The computations have been carried out for a range of initial diameter ratios $0.90 < \lambda_i < 1.05$ in which the equations of linear elasticity and the Reynolds equations may be expected to be reasonable approximations.

3. NUMERICAL RESULTS AND DISCUSSION

The solutions for rigid particles and numerical results obtained for elastic spheres are discussed below.

Truncated cones

The solution given in section 2 is valid for an arbitrary conical angle α provided the gap thickness h is small. The squeeze film effect that results can be seen simply as follows. The relation between particle velocity U and the mean velocity $\bar{V}$ at the upstream end of the

particle is given by [2.17]. Considering only the first term in the expansion in h we have

$$\bar{V} = \frac{U}{2}\frac{r_1^2 + r_2^2}{r_1^2} + O(h). \tag{3.1}$$

Using the continuity equation $\pi r_1^2 \bar{V} = \pi r^2 V$, the mean velocity V at any position s is:

$$V = \frac{U}{2}\frac{r_1^2 + r_2^2}{r^2} + O(h). \tag{3.2}$$

Equation [3.2] shows that $V < U$ at the upstream end $r = r_1$ but $V > U$ when $r = r_2$ at the downstream end of the particle. This shows that the fluid escapes from both ends due to squeezing effects. It is of interest to express [3.2] in terms of the leakback Q measured relative to axes fixed to the particle:

$$2\pi rQ = \pi r^2(U - V) = \pi U\left(r^2 - \frac{r_1^2 + r_2^2}{2}\right). \tag{3.3}$$

If one substitutes $r = r_1$ or $r = r_2$ in [3.3] the same absolute value of the discharge $2\pi rQ$ results but with opposite signs. This shows that equal amounts of fluid leave the gap at the two ends of the particle. Moreover, [3.3] shows that $Q = 0$ at $r = [(r_1^2 + r_2^2)/2]^{1/2}$.

While there is no restriction on the magnitude of α in the solutions for rigid truncated cones obtained in section 2, it is of interest to consider small α for which these solutions reduce to

$$2\pi r_1 Q_1 = -2\pi r_2 Q_2 = \pi L r_1 U\alpha + O(\alpha^2) \tag{3.4}$$

where L is the length of the particle and

$$\Delta p = \frac{2\mu U}{r_1 h^3} L^3 \sin^2\alpha + O(h^{-2}). \tag{3.5}$$

For fixed h, as $\alpha \to 0$ the terms of $O(h^{-3})$ and $O(h^{-2})$ in the asymptotic expansion of Δp approach zero and the terms of $O(h^{-1})$ become predominant in this expansion. These terms of $O(h^{-1})$ cannot be determined accurately by using the one-dimensional Reynolds equation. However, as $\alpha \to 0$ for h fixed, it is reasonable to assume that the results will approach the solutions for the flow of circular cylinders in cylindrical tubes for which the leading term in the asymptotic expansion of Δp is $2\mu U/h$ (see Chen & Skalak 1970).

Rigid spheres

For the rigid spheres, the effects of squeezing motion can be illustrated most clearly by comparing pressure curves for different cone angles, α. Figure 4 shows the pressure vs axial coordinate curves for $\alpha = 0$, 1, 2 and 3°. Equations [2.43]–[2.45] (the equations developed to treat the elastic particle problem) are numerically integrated for the spherical shape to obtain these curves. For all these curves λ_i is equal to 0.99. The pressure for steady-state problem ($\alpha = 0$) is symmetric with respect to origin. For $\alpha \neq 0$, there is a significant increase of pressures in the vicinity of origin and curves become more asymmetric with increasing α. These trends may be readily explained by considering the axisymmetrical squeeze film problem involving a stationary rigid sphere in a cylindrical tube in which the tube walls are assumed to have a radial velocity $U \sin\alpha$. The integration of Reynolds equation in one-dimension [2.19], using $Q = 0$ at $h = h_0$ and $p = 0$ at the upstream end of the particle yields:

$$p_{max} \approx \frac{6\mu a U \sin\alpha}{h_0^2} \quad \text{at} \quad h = h_0. \tag{3.6}$$

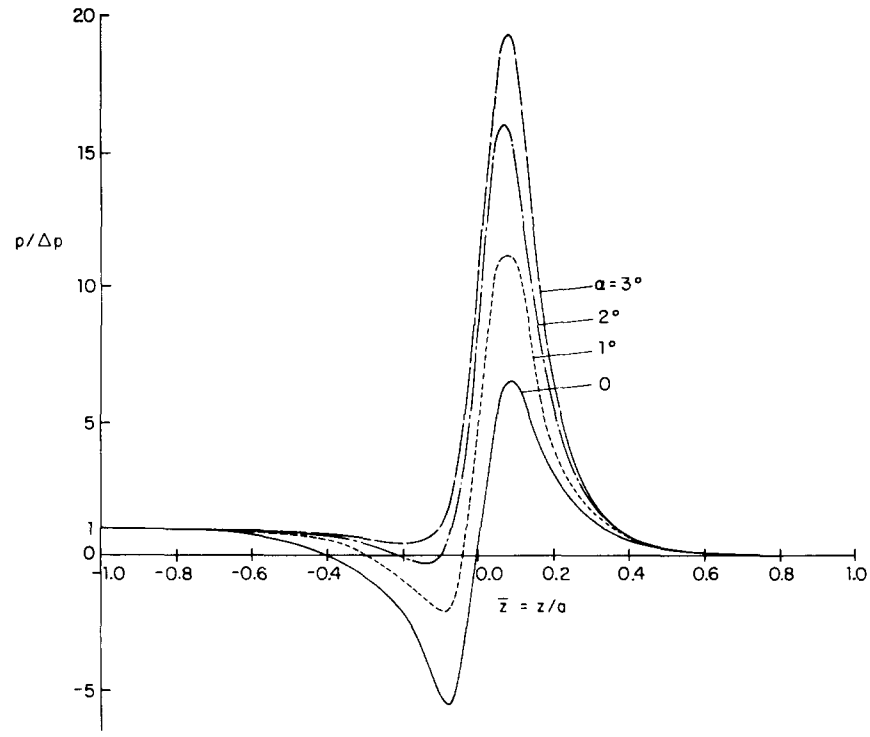

Figure 4. Comparison of pressure curves for $\alpha = 0$, 1, 2 and 3°. The particle in each case is a rigid neutrally buoyant sphere.

This term approximates the effects of squeezing motion on the pressures for the case of a tapered tube with taper angle α. The integration of the Reynolds equation for a neutrally buoyant sphere translating in a straight tube ($\alpha = 0$) yields:

$$p_{max} \approx \frac{3\sqrt{(3)}\mu a U}{4\sqrt{(2)}R_0^{1/2}h_0^{3/2}} \quad \text{at} \quad h = \frac{4}{3}h_0 \qquad [3.7]$$

where we have used $Q = \frac{2}{3}Uh_0$. For small h_0, with α small but nonzero, the term given by [3.6] becomes predominant with respect to [3.7]. As α increases the location of maximum pressure moves towards the origin where terms due to squeezing motion attain their maximum.

For the flow of neutrally buoyant rigid spheres in cylindrical tubes, V and Δp are given by (Bungay & Brenner 1973):

$$V = U\left(1 - \frac{4}{3}\frac{h_0}{R_0}\right) + O(h_0^2) \qquad [3.8]$$

$$\Delta p = \frac{4\sqrt{(2)}\pi}{h_0^{1/2}}\frac{\mu U}{r_0^{1/2}} + O(1). \qquad [3.9]$$

The terms in the asymptotic expansion of Δp due to the squeezing motion have a significant contribution to pressure drop as can be seen by comparing [2.37] with [3.9]. For a fixed α (however small), the ratio of pressure drops for the case of straight tube to that for the tapered tube approaches zero as $h_0 \to 0$. There is also a range of α and h_0 for which terms of $O(\alpha^2 h_0^{-3/2})$ and $O(h_0^{-1/2})$ have the same order of magnitude.

The Reynolds equation in one-dimension used in this analysis does not accurately determine the terms of $O(h_0^{-1/2})$. The Reynolds equation developed for axisymmetric problems [2.44], [2.43] and [2.45] are numerically integrated to investigate this range of h_0 and α. The results are shown in figure 5. The solid lines in this figure give $\Delta p' = \Delta p/(16\mu V a/r_0^2)$ vs λ_i curves for

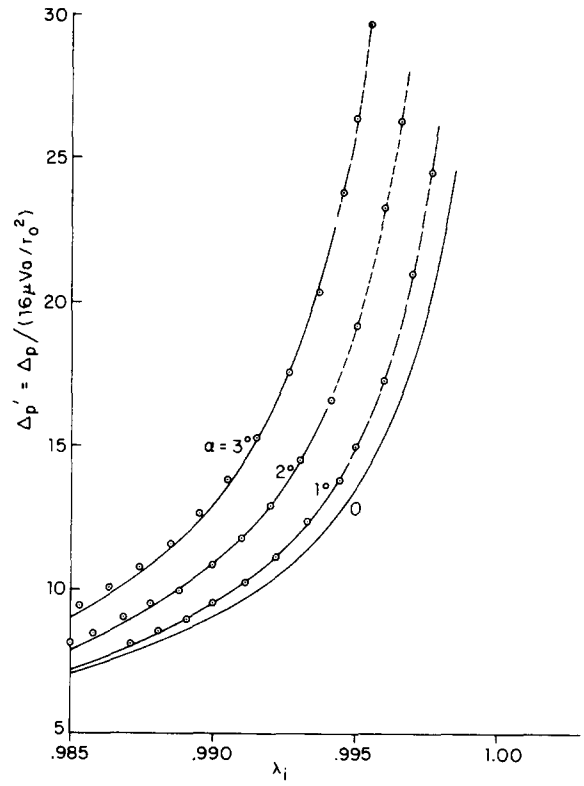

Figure 5. Dimensionless pressure drop $\Delta p'$ vs initial diameter ratio λ_i for several values of taper angle α. The solid lines are obtained by numerically integrating the Reynolds equation. The broken lines and points indicated by small circles are obtained by adding $\Delta p'$ calculated numerically for $\alpha = 0$ and $\Delta p'$ obtained using [2.9]. The particles are neutrally buoyant rigid spheres.

$\alpha = 0,1, 2$ and 3° computed by numerical integration. Also shown are $\Delta p' = \Delta p/(16\mu Va/r_0^2)$ vs λ_i curves (indicated by small circles and broken lines) obtained by adding $\Delta p'$ for $\alpha = 0$ obtained numerically to $\Delta p'$ computed using [2.37]. There is a very good correlation between these curves as can be seen from this figure. It follows that Δp computed by adding the results of [3.9] and [2.37] may be used as an acceptable approximation for small α and when $O(\alpha^2 h_0^{-3/2})$ and $O(h_0^{-1/2})$ terms in the asymptotic expansion of Δp are of the same order of magnitude.

Elastic incompressible spheres

The results for elastic incompressible spheres are obtained by applying the numerical procedure described in section 2 for several different values of $\Delta\bar{p}$ and α. Equations [2.43]–[2.46] are solved to determine A, C, $\bar{u}_i$ and $\bar{v}_i$. These results are obtained for the range $0.9 < \lambda_i < 1.05$ by incrementing the dimensionless time. When Δp, μ and G are specified, these nondimensional results can be used to determine the dimensional variables as functions of time by using the definitions of dimensionless variables given in section 2.

In discussing the numerical results, the shapes of deformed particles and pressure curves will be illustrated first. In figure 6 the pressure is shown as a function of $\bar{z}$ for $\Delta\bar{p} = 0.1$, $\lambda_i = 1.04$ and $\alpha = 0$, 1 and 3°. This fairly high value of $\Delta\bar{p}$ implies that either G is small (soft particle) or Δp is large. The minimum and maximum pressures tend to increase slightly with increasing α; otherwise, the curves are similar and close to each other. The behavior of these curves is in contrast with the pressure curves for rigid particles shown in figure 4. For rigid spheres with $\lambda_i = 0.99$ the maximum pressure increases by a factor of about four as α varies between 0 and 3°. The dependence of pressure curves on α is weaker in the case of a soft particle because of significant particle deformations and velocities at the surface of the particle.

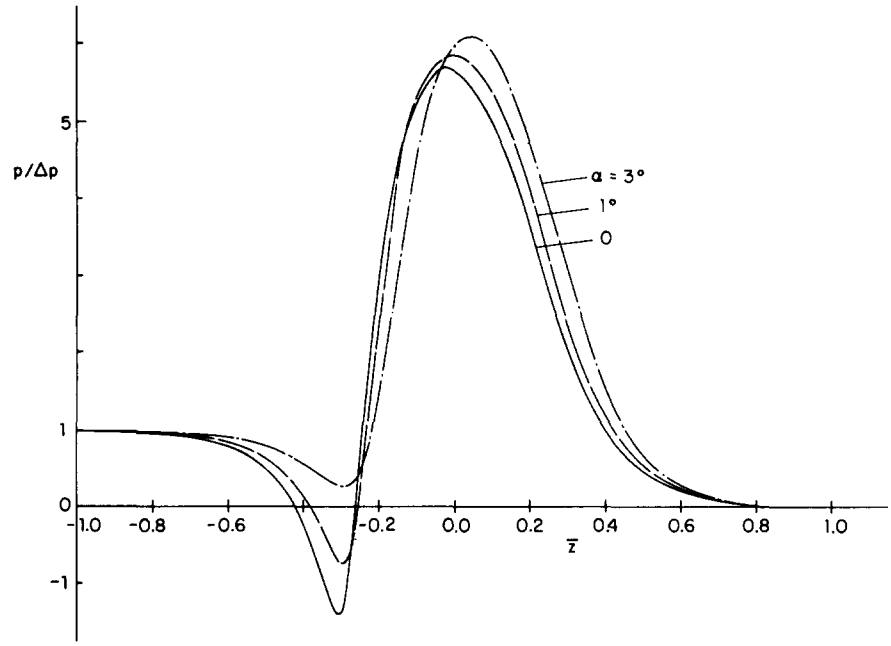

Figure 6. Pressure curves for $\lambda_i = 1.04$, $\Delta\bar{p} = 0.01$ and $\alpha = 0$, 1 and 3°. The particle is an elastic incompressible sphere.

For stiffer particles or lower values of Δp, the behavior of pressure curves is closer to that of rigid spheres shown in figure 4.

Figure 7 shows the gap thicknesses and particle deformations for the same values of λ_i, $\Delta\bar{p}$ and α used for figure 6. The $\bar{z}$ axis may be regarded as the location of the tube wall in figure 7 to interpret the gap thickness curves $h' = h/a$ and the curves for original particle shapes. The minimum gap thickness increases with increasing α. In the rest of the lubrication region h' curves for different α values are very close to each other and show little variation with respect to $\bar{z}$. The locations of minimum fluid film thickness and maximum deformation move towards the downstream end of the particle as α increases.

When h is small compared to the elastic displacements, the pressures cannot vary significantly with α from considerations involving elasticity of the particle alone. This partly

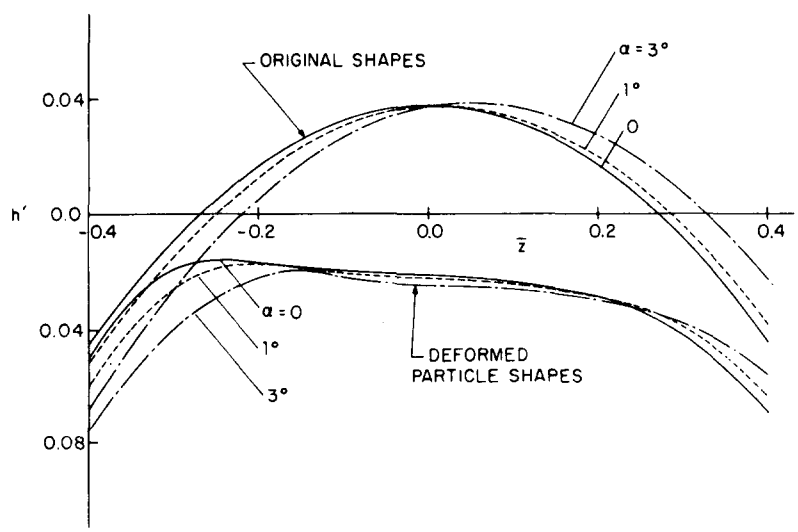

Figure 7. The original and deformed particle shapes for $\lambda_i = 1.04$, $\Delta\bar{p} = 0.01$, $\alpha = 0$, 1 and 3°. The particle is an elastic incompressible sphere.

explains the difference between the pressure curves for rigid spheres (figure 4) and elastic spheres (figure 6). For elastic particles the values of the velocities along the particle surface are comparable to $U \tan \alpha$. This is another reason that the effect of α is less for soft particles compared to rigid spheres. The magnitude of pressures is further reduced by the increase of film thickness for soft particles as α increases as can be seen from figure 8.

Figures 8(a)–(c) give the final diameter ratio λ_f (ratio of the initial particle radius to the maximum radius of the deformed particle) as a function of λ_i for several constant values of $\Delta\bar{p}$ and $\alpha = 0$, 1 and 3°. The value of λ_f is $\lambda_f = (1 - h_0')$ where $h_0' = h_0/r_0(0)$ and h_0 is the minimum gap thickness. The h_0' is given by the difference between the line $\lambda_f = 1$ and λ_f curve for each $\Delta\bar{p}$. The difference between 45° line and λ_f curves gives approximately the deformation that takes place at the point where minimum film thickness occurs. Comparison of λ_f curves for $\alpha = 0$, 1 and 3° shows that minimum fluid film thickness increases as α increases. This is due to increase of pressures caused by squeezing effects.

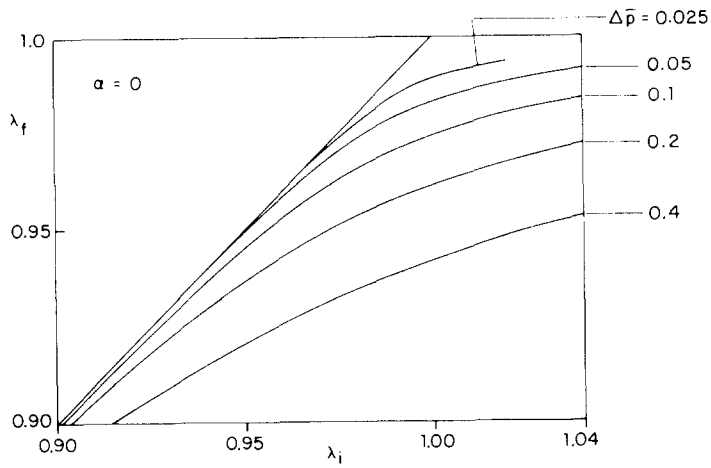

Figure 8(a).

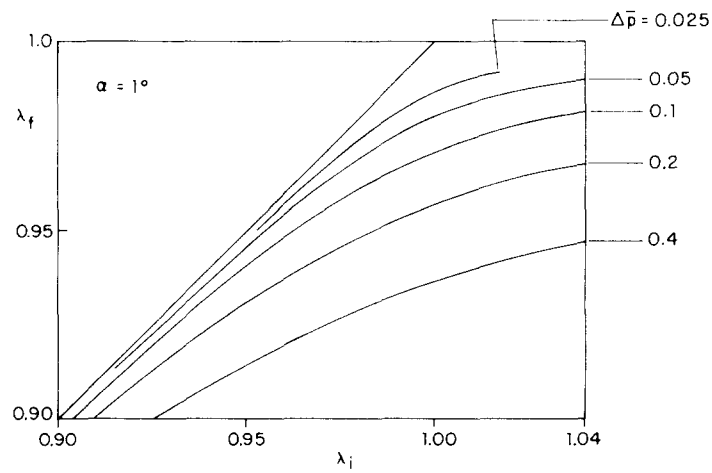

Figure 8(b).

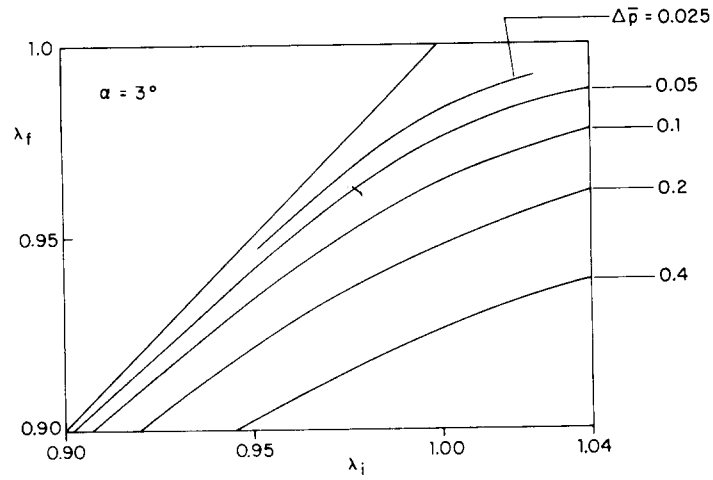

Figure 8(c).

Figure 8. Each set of curves shows final diameter ratios λ_f vs the initial diameter ratios λ_i for elastic, incompressible spheres. (a) $\alpha = 0$ (straight tube, steady flow), (b) $\alpha = 1°$, (c) $\alpha = 3°$.

Figures 9(a) and 9(b) give the ratio of maximum radial velocity v at the particle surface to radial velocity of tube wall ($U \tan \alpha$) as a function of λ_i and $\Delta\bar{p}$ for $\alpha = 1$ and 3°. The absolute value of v, for fixed μ and G, decreases as Δp and/or α decreases. However, the dimensionless velocity $v/(U \tan \alpha)$ vs λ_i curves for different $\Delta\bar{p}$ cross each other. For smaller values of λ_i, the lubrication pressures are more or less independent of G but vary with Δp. The radial velocity v is inversely proportional to G. So $(v/U \tan \alpha)$ varies with $\Delta\bar{p}$. For higher values of λ_i, the relative positions of the curves change (figures 9a, b). For stiffer particles the gap width is much smaller compared to softer particles as can be seen from figure 8(a)–(c). In the limit of very small gap thickness, the radial velocity v much approach $U \tan \alpha$. Accordingly the value of $v/(U \tan \alpha)$ becomes greater for smaller values of $\Delta\bar{p}$ which results in smaller gap thicknesses.

For a fixed $\Delta\bar{p}$, the curves $v/(U \tan \alpha)$ vs λ_i for $\alpha = 1°$ compared to $\alpha = 3°$ exhibit a similar behavior. Figures 8(a) and 8(b) show that the minimum gap width is smaller for smaller α when $\Delta\bar{p}$ is fixed, thus leading to higher values of relative velocity $v/(U \tan \alpha)$ as can be seen by comparing $\Delta\bar{p} = 0.025$, $\alpha = 1$ and 3° curves in figures 9(a) and (b).

The dimensionless pressure drop $\Delta p' = \Delta p/(16\mu Va/r_0^2)$ vs initial diameter ratio λ_i curves for $\alpha = 0$, 1 and 3° are shown in figure 10. The differences between $\Delta p'$ curves for different values of α at fixed $\Delta\bar{p}$ are small for large $\Delta\bar{p}$. These differences are greatest for rigid spheres. The behavior of these curves can be understood by comparing the curves for rigid and soft elastic spheres. For rigid spheres there is no velocity at the particle surface and the terms due to squeezing motion in the asymptotic expansion for $\Delta p'$ [2.9] become increasingly important as α increases. For the case of soft elastic particles the time derivative of h is much smaller than $U \tan \alpha$ (see figures 9a and b). The pressure drop is further reduced by an increase of h for increasing α. Therefore, the differences between $\Delta p'$ curves for different α values are small for soft elastic particles. The majority of curves lie between these two extreme cases.

Figure 11 shows the dimensionless velocity $U' = U/(a\Delta p/\mu)$ vs λ_i curves for several values of $\Delta\bar{p}$ and α. All the curves for different $\Delta\bar{p}$ values approach each other as λ_i decreases (when the deformations are small compared to gap thicknesses). There is a considerable decrease of particle velocity as it translates in the direction of decreasing tube radius for all $\Delta\bar{p}$ and α. The effect of α is more significant for rigid spheres. For example, a comparison of the values of U' for $\lambda_i = 0.995$, $\alpha = 0$ and 3° shows that rigid spheres translate twice faster in straight tubes than tapered tubes with taper angle $\alpha = 3°$ for $\lambda_i = 0.995$. This difference in velocities (for fixed λ_i) is much reduced for softer elastic particles (i.e. for $\Delta\bar{p}$ large).

The successive approximation procedure described in section 2 is not convergent when h_0' is

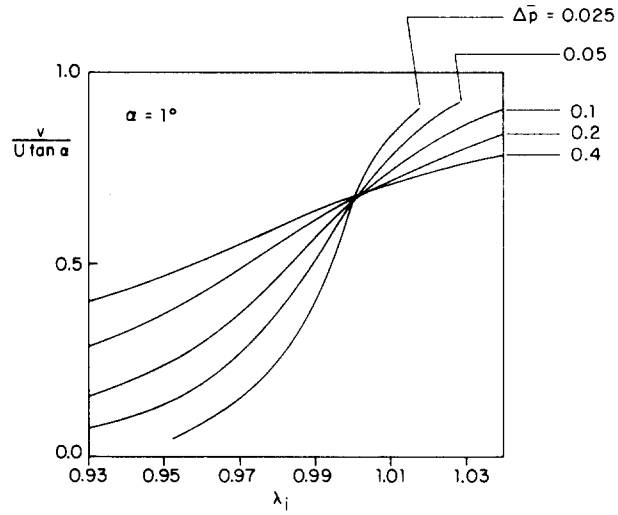

Figure 9(a).

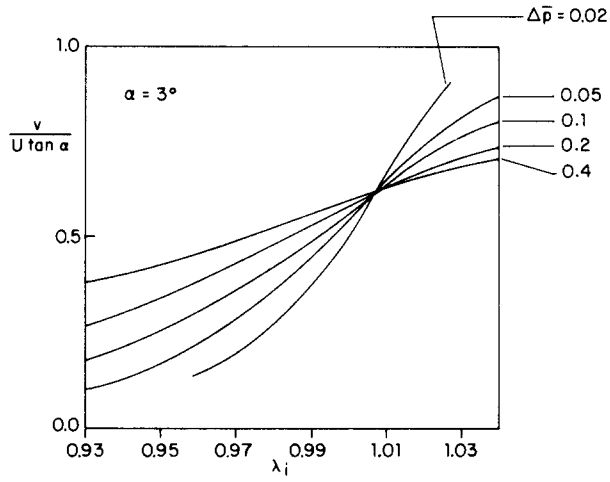

Figure 9(b).

Figure 9. The dimensionless maximum surface velocity of the particle ($v/U \tan \alpha$) as a function of λ_i and $\Delta\bar{p}$. (a) $\alpha = 1°$, (b) $\alpha = 3°$.

less than 0.005 (or $\lambda_f > 0.995$). It was therefore not possible to investigate numerically the limiting situations involving very small particle velocities. The contact theory of elasticity has been successfully applied in lubrication literature (see Desmond 1972) in these limiting cases for which (i) U is small, (ii) a is slightly greater than r_0, and (iii) deformations are much larger compared to the thickness of the lubrication film. Application of contact theory of elasticity to axisymmetric particle flows to develop analytical relations between Δp, U and some material and geometrical variables will be the subject of a future publication.

Acknowledgements—The authors would like to thank Messrs. C. C. Hsiung and N. Grossman who checked part of section 2 and provided help in computational work. This work was supported by U.S. National Institutes of Health under Program Project HL-16851.

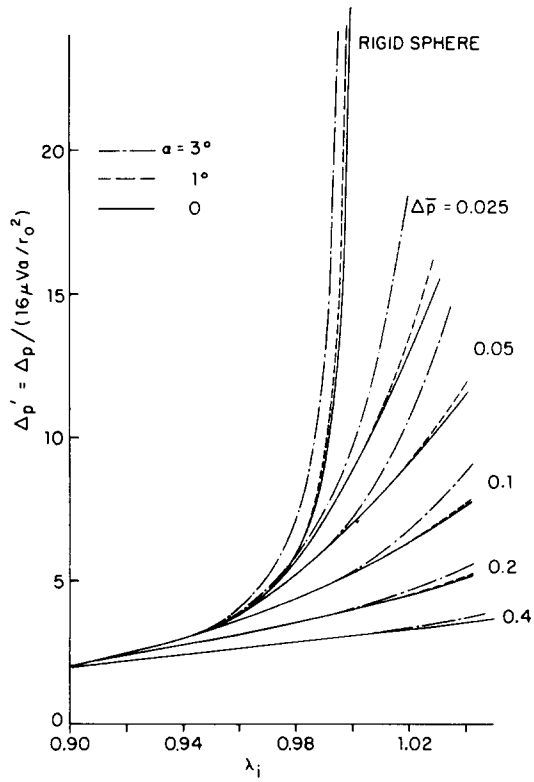

Figure 10. The dimensionless pressure drop $\Delta p'$ vs initial diameter ratio λ_i for several constant values of $\Delta\bar{p}$ and $\alpha = 0$, 1 and 3°.

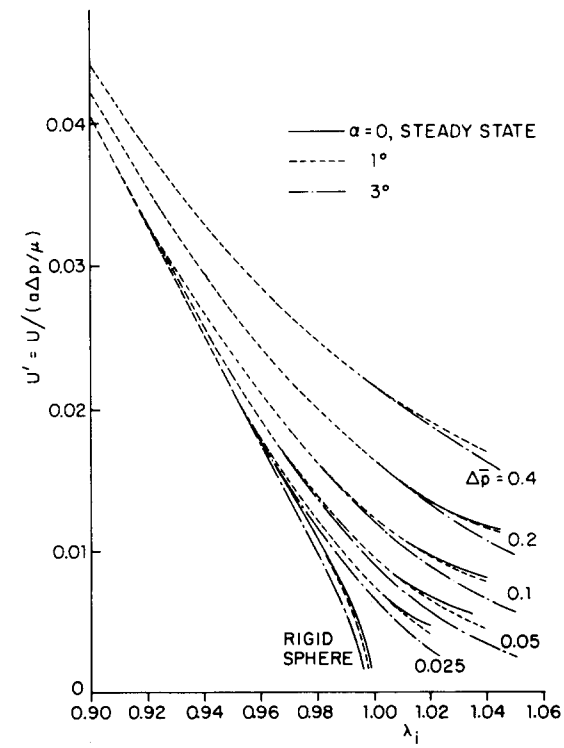

Figure 11. The dimensionless particle velocity U' vs λ_i curves for constant values of α and $\Delta\bar{p}$.

REFERENCES

ARCHIBALD, F. R. 1956 Load capacity and time relations for squeeze films. *Trans. ASME* **78**, 29–35.

BUNGAY, P. M. & BRENNER, H. 1973 The motion of a closely-fitting sphere in a fluid filled tube. *Int. J. Multiphase Flow* **1**, 25–56.

CAMERON, A. 1966 *The Principles of Lubrication*, p. 173. Wiley, New York.

CHEN, T. C. & SKALAK, R. 1970 Stokes flow in a cylindrical tube containing a line of spheroidal particles. *Appl. Sci. Res.* **22**, 403–441.

DESMOND, F. M. 1972 *The Friction and Lubrication of Elastomers*, 1st Edn. Pergamon Press, New York.

FITZ-GERALD, G. M. 1969 Mechanics of red-cell motion through very narrow capillaries. *Proc. R. Soc.* **B174**, 193–227.

GOLDSMITH, H. L. & SKALAK, R. 1975 Hemodynamics. In *Annual Review of Fluid Mechanics*, Vol. 7, pp. 213–247.

LAMB, H. 1945 *Hydrodymanics*, 6th Edn. Dover, New York.

LOVE, A. E. H. 1944 *A Treatise of the Mathematical Theory of Elasticity*, 4th Edn. Dover, New York.

TÖZEREN, H. & SKALAK, R. 1978 The steady flow of closely fitting incompressible elastic spheres in a tube. *J. Fluid Mech.* **87**, Part 1, 1–16.